applied optics

Design and optimization for main support structure of a large-area off-axis three-mirror space camera

Lei Wei,[1,2] Lei Zhang,[1,3,*] Xiaoxue Gong,[1,2] and Dong-mei Ma[1,3]

[1]Changchun Institute of Optics, Fine Mechanics and Physics, Chinese Academy of Sciences, Changchun 130033, China
[2]University of Chinese Academy of Sciences, Beijing 100039, China
[3]Chang Guang Satellite Technology LTD Co., Jilin Changchun 130000, China
*Corresponding author: 18686344285@163.com

Received 30 September 2016; revised 26 December 2016; accepted 26 December 2016; posted 6 January 2017 (Doc. ID 277868); published 31 January 2017

To ensure excellent dynamic and static performance of large-area, off-axis three-mirror anastigmat (TMA)-space cameras, and to realize a lighter weight for the entire system, a truss support structure design is applied in this study. In contrast to traditional methods, this paper adopts topology optimization based on the solid isotropic materials with penalization method on the truss structure design. Through reasonable object function and constraint choice, optimal topology results that have concerned the effect of gravity in the X, Y, and Z axis are achieved. Subsequently, the initial truss structure is designed based on the results and manufacturing technology. Moreover, to reduce the random vibration response of the secondary mirror and fold mirror without mechanical performance decline of the whole truss, a weighted optimization of truss size is proposed and the final truss structure is achieved. Finite element analysis and experiments have confirmed the reliability of the design and optimization method. The designed truss-structure camera maintains excellent static performance with the relative optical axis angle between the primary mirror and corresponding mirrors (secondary mirror and fold mirror) being less than 5.3 in. Dynamic performances, such as random and sinusoidal vibration responses, also met the requirements that the acceleration RMS value for mount points of the fold mirror should be less than 20 g and the primary frequency reached 97.2 Hz.

OCIS codes: (280.0280) Remote sensing and sensors; (280.4788) Optical sensing and sensors; (350.4600) Optical engineering; (350.5730) Resolution; (350.6090) Space optics.

https://doi.org/10.1364/AO.56.001094

1. INTRODUCTION

With the development of Earth remote sensing imaging technology, lightweight, large fields of view (LFOV), and high image resolutions are in high demand for space cameras. Therefore, off-axis three-mirror anastigmat (off-axis TMA) optical systems with these advantages have been used extensively in space cameras. However, off-axis TMA optical systems have also brought about great difficulties, such as main support structure design, optical system alignment during the development process owing to the characteristics of long focal distances, LFOV, and asymmetry [1].

This paper focuses on research into the main support structure design. It is well known that all the mirror subassemblies are assembled on the main support structure of a space camera, so that the main support structure has access to provide a fixed means of optical system installation to ensure that the optics remain relatively stable when located in space, which is the key to guaranteeing an accurate structural location and imaging quality for the optical elements. Therefore, appropriate design of high-stability main supporting structures is the key to satisfying the demands of optical systems [2–4].

So far, thin-walled cylindrical structures and truss structures have been mainly adopted as camera main support structures; e.g., the main support structure of the QuickBird 2 satellite with 8.8 m focal length launched in 2001 employs a cylindrical structure [5]. In contrast, HUBE, ALOS-3 [6–8], Hi-RISE [9], etc., adopt a truss structure. Considering the influence caused by weight, material processing manufacturability of the space camera researched in this paper, a truss structure is employed as the main support structure.

Space cameras usually experience complex dynamic environments in orbit and during launch. The stiffness and strength of a truss structure can directly guarantee the mechanical performance of a space camera in such an environment [10].

Therefore, lots of researchers around the world have studied the truss support structure of space cameras for decades. For example, Atwood and O'Brien have developed an adjustable truss structure for the Schmidt space camera, which can make optical alignment adjustable to reduce the influence of thermal load [11]. Imai and co-workers have developed a truss support structure for the ALOS-3 space camera [6–8], which has an off-axis TMA optical system. Xin from China has designed and studied the truss support structure of an off-axis TMA long focal length space camera [12,13]. However, research into the optimization of space camera truss support structures is almost entirely based on mode frequency or structural stiffness. The dynamic performance index of a space camera also includes the natural frequency, the frequency responses to acceleration, random vibration responses, etc. Traditional research into optimization of space cameras is not optimal. To improve present research, this paper includes influences of truss rod cross-section dimensions on the random vibration response of parts of the key payload installation into account after a brief truss structure is determined, and determines an optimization method that is based on the acceleration RMS value (GRMS) of random vibrations. In this way, the author of this paper has obtained a main truss support structure with excellent dynamic performance with sufficient dimensional stability for the camera structure. After finite element (FEM) analysis and experimental verification, the main truss support structure researched in this study has met the requirements of a space camera under development.

2. MAIN SUPPORT STRUCTURE DESIGN OF SPACE CAMERA

The off-axis TMA optical system studied in this paper is shown in Fig. 1. The distinct characteristics of this off-axis TMA space camera are a high resolution and LFOV, which make the mirror heavier and larger as a result. In particular, the fourth mirror component weighs 42 kg and is more than 1000 mm long. The interval distance between the first mirror and secondary mirror researched in this paper reaches up to 1500 mm. The requirements of positional accuracy for all the optical components are shown in Table 1.

In contrast to the traditional Rayleigh method used to optimize the angle of the truss rod [14,15], topology optimization of the main support structure based on solid isotropic material with penalization (SIMP) [16–19] was applied in this study

Table 1. Requirements of Optical Tolerance

	Eccentric			Tilt		
Mirror	**ΔX(mm)**	**ΔY(mm)**	**ΔZ(mm)**	**$\theta X('')$**	**$\theta Y('')$**	**$\theta Z('')$**
M1	Datum	Datum	Datum	Datum	Datum	Datum
M2	0.03	0.03	0.04	13	13	20
M4	none	none	none	30	30	none

using the FEM software Patran. According to the topology optimization results, an initial truss structure for the space camera is given in Fig. 4.

The optimization model can be expressed as follows:

Optimization objective:

$$\text{Minimize: } C_s = \gamma C_x + \eta C_y + \kappa C_z. \quad (1)$$

Constraints:

(1) The main support structure must weigh no more than M (kg).

(2) The displacement of mass points M2 and M4 under gravity loads in the X, Y, and Z directions should be no more than 0.03 mm, respectively.

In this model, C_s is the optimization objective that is weighted by C_x, C_y, and C_z. Note that C_x, C_y, and C_z are the compliance functions of the whole structure under gravity in the X, Y, and Z directions, respectively. γ, κ, and η are weighting factors (this paper selects 0.33 for γ, κ, and η).

In accordance with the optical system shown in Fig. 1, we established the FEM model of the main support structure of a researched space camera, as shown in Fig. 2. The boundary conditions and constraints of the FEM model are given as follows:

1. M1, M3, and the focal surface are all mounted on the rear frame while M2 and M4 are mounted on the front frame. The design domain (shown in Fig. 2) is the space between the front frame and the rear frame with the light region removed.
2. M2 and M4 are equivalent to the mass point and connected with the entire FEM model by use of a rigid connection, RBE2.
3. Fix the bottom of the FEM model.
4. The material properties of the entire FEM model in Fig. 2 are shown in Table 2.

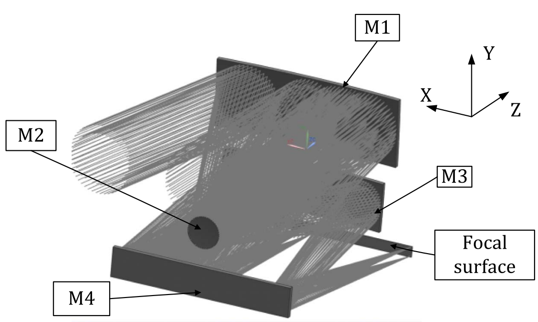

Fig. 1. Optical system layout.

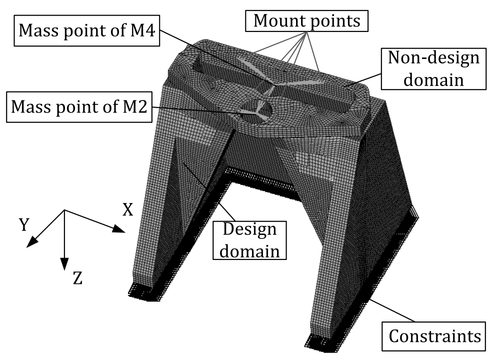

Fig. 2. Initial FEM model of main support structure.

Table 2. Material Properties

Density(g/cm^3)	Elastic Modulus (Mpa)	Poisson's Ratio
1.8	65000	0.33

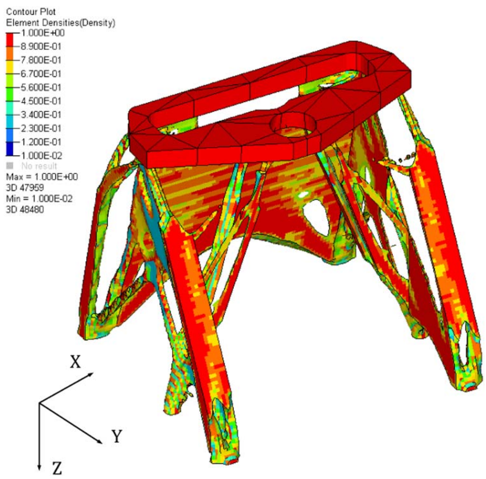

Fig. 3. Topology optimization result.

After a large number of iterations of the optimization calculation, we obtained optimal material distribution results for the optimization model under a gravity load in three directions (X, Y, Z). Since topology optimization is based on the SIMP method, which takes the density of every FEM model element as the optimization variable, the final result given in Fig. 3 is shown in the form of a density cloud image. The higher the area density is, the more significant the area is. All the trusses are designed based on an area with high density.

The lightweight result that is obtained by topology optimization cannot be used directly in practical applications. Therefore, we designed the truss structural form based on the optimization results combined with actual processing technology. The final structure is shown in Fig. 4.

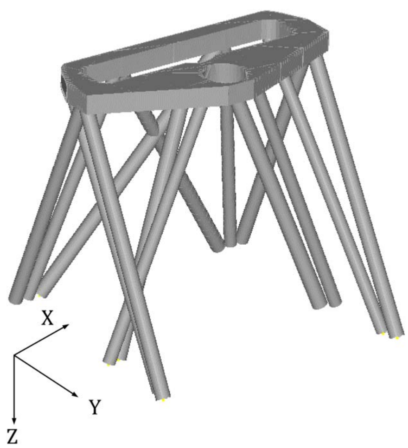

Fig. 4. Main support structure after optimization.

3. OPTIMIZATION OF TRUSS ROD CROSS SECTION BASED ON RANDOM VIBRATION RESPONSE

A. Theoretical Analysis of Random Vibration Response

Since random vibration loads are made up of various instantaneous vibration excitations, it is hard to find regularity in the instantaneous vibrations during the random vibration test. Generally, through statistics such as the RMS value or power spectral density (PSD) within a loading cycle, research into the random vibration response of space cameras is available [20–22].

The kinetic equation for a single degree-of-freedom for a forced vibration can be expressed as

$$m\ddot{y} + c\dot{y} + ky = x(t), \tag{2}$$

where m, c, and k are the mass, damping and stiffness, respectively, and $x(t)$ is the excitation function.

The response and excitation functions are given in the form of complex exponential functions that can be expressed as follows:

$$x(t) = \frac{1}{2\pi}\int_{-\infty}^{\infty} X(\omega)e^{i\omega t}\mathrm{d}t, \tag{3}$$

$$y(t) = \frac{1}{2\pi}\int_{-\infty}^{\infty} H(\omega)X(\omega)e^{i\omega t}\mathrm{d}t. \tag{4}$$

Substituting Eqs. (3) and (4) into Eq. (2) gives Eq. (5):

$$[-\omega^2 m + i\omega c + k]H(\omega)X(\omega)e^{i\omega t} = X(\omega)e^{i\omega t}. \tag{5}$$

The transfer function of the system can be expressed as

$$H(\omega) = \frac{1}{k - m\omega^2 + ic\omega}, \tag{6}$$

$$|H(\omega)| = \frac{1}{k\sqrt{(1 - s^2)^2 + (2\varsigma s)^2}}. \tag{7}$$

The output power spectral density function is

$$S_y(\omega) = |H(\omega)|^2 S_x(\omega). \tag{8}$$

The mean-square value function of output is

$$\psi_y^2 = \int_{-\infty}^{\infty} S_y(\omega)\mathrm{d}\omega = \frac{1}{2\pi}\int_{-\infty}^{\infty} |H(\omega)|^2 S_x(\omega)\mathrm{d}\omega, \tag{9}$$

where $S = \omega/\omega_n$, $\zeta = c/2\ (\mathrm{km}^{1/2})$, and $S_x(\omega)$ is the input PSD function. It can be ascertained from Eqs. (4) and (8) that the output PSD functions, $S_y(\omega)$, and ψ_y^2 are only related to the input PSD function $S_x(\omega)$.

Substitution of $S = \omega/\omega_n$ and $\zeta = c/2\ (\mathrm{km})^{1/2}$ into Eq. (7) gives

$$|H(\omega)| = \frac{1}{\sqrt{k^2\left(1 - \left(\frac{\omega}{\omega_n}\right)^2\right)^2 + \frac{k}{m}\left(\frac{c\omega}{\omega_n}\right)^2}}. \tag{10}$$

It can be inferred from Eq. (8) that the output RMS, ψ_y^2, is proportional to $|H_{(\omega)}|$ for a single degree-of-freedom system. According to Eq. (9), when ω_n is determined, $|H_{(\omega)}|$ is proportional to K, the stiffness matrix of partial structure. Therefore, when the natural frequency is determined for the entire structure, the stiffness increase of partial areas can decrease the RMS of the acceleration random response in the corresponding partial areas.

According to the above theories, this paper finds out that the rigidity reinforcement of key areas can reduce the GRMS of the corresponding areas. However, the stiffness of unimportant regions needs to be balanced to keep the overall frequency of the whole structure unchanged.

B. Optimization and Analysis of the Results

Improving the fundamental frequency of the space camera can avoid the rocket's natural frequency, which is a good way to reduce the acceleration response of the camera. However, random vibration loads can be described by the acceleration spectrum during launch, the frequency of which ranges between 20 and 2000 Hz, so random vibration response may not be reduced by improving the modal frequency of the camera. Application of a flexible vibration isolator is another possible way to reduce the random vibration response, but the pointing accuracy of the space camera will decline, which is undesirable. Therefore, it is of great importance to research truss support structures that can withstand the complex dynamic environment during the rocket's launch and meet the requirements of a camera ground test. This paper proposes a method to optimize the main truss support structure that minimizes the root mean square value of the random vibration acceleration response (GRMS) at the mounting point of the mirror component under the constraints of the total mass and modal frequency.

The FEM model of the camera truss support structure has been established and is shown in Fig. 5. An excessive moment of inertia would bring out an excessive dynamic response of both the M2 and M4 components in the front of the support structure during the rocket launch. When a dynamic response, such as acceleration response, stress etc., exceeds the system limits, plastic deformity, or even destruction of the optical support structure, will eventually occur. To avoid this situation, we established the objective function that requires a minimal GRMS for the random vibration response of the M4 and M2 component mount points in the rocket launch direction (z direction). The optimization is given below:

Objective function:

$$\text{Minimize: } D = \alpha b_1 + \beta b_2. \tag{11}$$

Constraints:

$$\begin{aligned} M &\leq N(\text{kg}) \\ f_1 &\geq 110\ \text{Hz} \\ 25\ \text{mm} &\leq r_i \leq 45\ \text{mm} \\ 4\ \text{mm} &\leq T^i_{\text{rod}} \leq 10\ \text{mm}\,(i = 1, 2, 3, 5, 6, 7, 8). \end{aligned} \tag{12}$$

Design Variable:

$$r_i,\ T^i_{\text{rod}\ i},$$

where D is the optimization objective weighted by b1 and b2, b1 is the GRMS of the M4 mounting point, b2 is the GRMS of the M2 mounting point, and α and β are weighting factors (this paper selects 0.65 for α and 0.35 for β). f_1 is the primary frequency of the space camera; T^i_{rod} is the thickness of the ith truss rod, the limit of which is 4 mm, as the minimum wall thickness of the rod is based on the actual processing technology; M is the mass of the FEM model for design domain; N is the upper bond of the whole space camera mass variable range since overweight of the whole truss structure is not permitted; r_i is the inner diameter of the ith rod.

After multiple iterations, the optimization function has converges. The optimization results for varying rod sizes are shown in Table 3. Figures 6 and 7 are the iteration histories of the primary frequency and the optimization object of the space camera, respectively, including the primary frequency of the space camera, the GRMS of the M4 mounting point, the GRMS of the M2 mounting point, and D.

Since the optimization object involves the GRMS of both the M2 mounting point and the M4 mounting point, rod 2, which is located just below these mounting points, becomes the biggest and thickest among all the rods. This can be easily explained due to the random vibration response theory

Table 3. Rod Sizes After Optimization

	Rod 1	Rod 2	Rod 3	Rod 5	Rod 6	Rod 7	Rod 8
r_i (mm)	30.2	34.2	29.8	37.2	30.4	27.2	29.4
T^i_{rod} (mm)	8.4	10	9.8	4.8	5.3	6.2	7.4

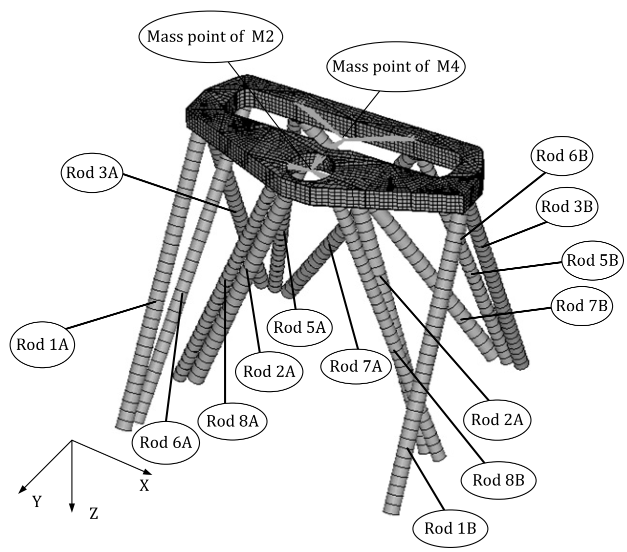

Fig. 5. Finite element model of the truss support structure.

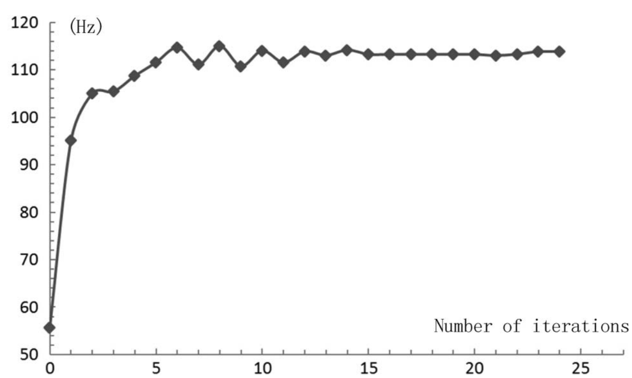

Fig. 6. Iteration history of the primary frequency of the space camera.

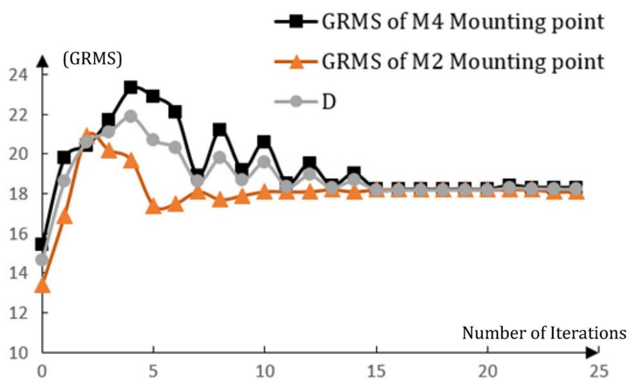

Fig. 7. Iteration history of the optimization object.

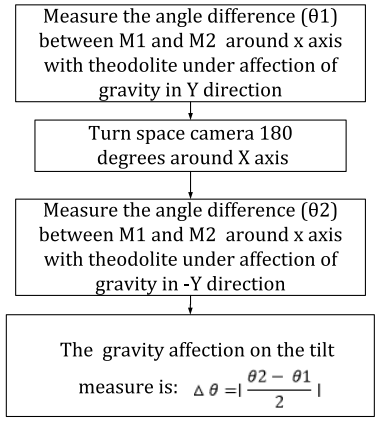

Fig. 9. Detection processes.

mentioned in Section 3.A. An increase of the dimensions of rod 2 includes the increase of the M2 and M4 support stiffness, which, in turn, will decrease their GRMS values. Meanwhile, the sizes of several other, unimportant rods become relatively small to keep the natural frequency of the whole structure unchanged.

4. FINITE ELEMENT ANALYSIS AND EXPERIMENTAL VERIFICATION

In order to verify the feasibility of the design for the main truss support structure and the effectiveness of the optimization method, we carried out a finite element simulation, static stability test, and vibration test on the whole space camera. Figure 8 gives the FEM model of the whole space camera.

A. Static Stability Finite Element Analysis and Test

The assembly and detection processes of the researched space camera are conducted on the ground with the optical axis horizontal (along the Z direction); the direction of gravity coincides with the Y direction of the camera during the process. Only if the position accuracy of the space camera optical components meets with the requirements given in Table 1, can the camera work sufficiently well. Therefore, the truss support structure, with a good dimensional stability, must overcome the effect caused by gravity in the Y direction.

To ensure the feasibility of the designed model, an FEM static stability analysis and on-ground static stability detection experiments of the model were conducted. The detection processes are illustrated in Fig. 9 and the testing field is shown in Fig. 10. The FEM analysis results and experimental results are all listed in Table 4.

At present, it is hard to perform gravity-free ground detection, so it is difficult to find the real position of the camera optical axis. To detect the effect of gravity on the camera, the author has designed a detection method shown in Fig. 9 that can detect the gravity effect on the camera indirectly. The testing field of step 1 in Fig. 9 is shown in Fig. 10 (testing field of step 3 is almost the same).

It is clear from the data presented in Table 4 that a relatively significant error occurs in θY, but it is much smaller than that of θX. This is because the true tilt of θY may be so small that minute environmental temperature fluctuation (20 ± 3°C, with the 22×10^{-6}/°C thermal expansion of Al) and errors caused by the operation will bring about a relatively large effect. It can be inferred from Fig. 10 that what affects θX most is the gravity, since the direction is in the normal plane of θX, so a

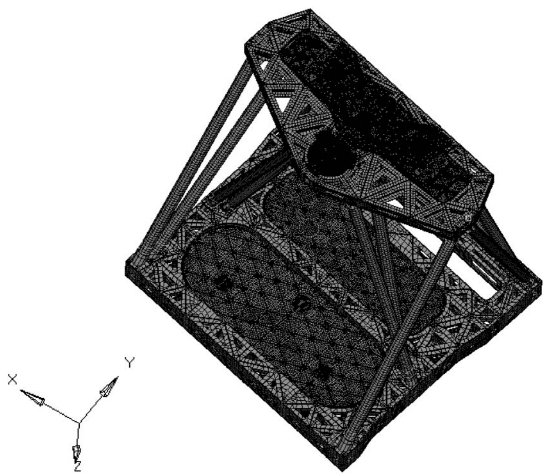

Fig. 8. FEM model of the whole space camera.

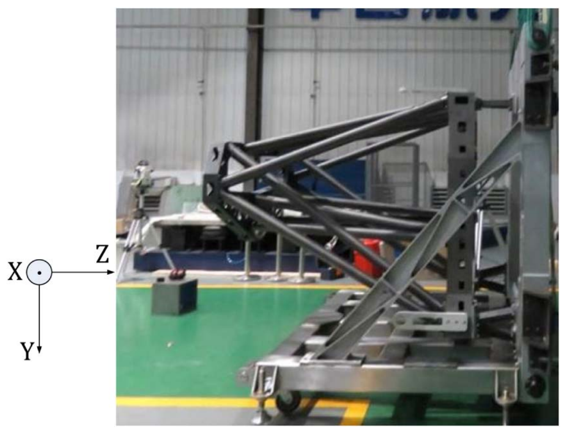

Fig. 10. Static stability testing field (camera assembled on aluminum testing frock).

Table 4. Comparison Between Experiment and Analysis Data

M1		The Tilt and Eccentricity of M2 Relative to M1		
		Analysis	Experiment	Requirement
$\theta X('')$	Datum	5.3	4.32	13
$\theta Y('')$	Datum	0.075	1.17	13
$\theta Z('')$	Datum	2	—	20
ΔX (mm)	Datum	0.007	—	0.03
ΔY(mm)	Datum	0.00038	—	0.03
ΔZ(mm)	Datum	0.033	—	0.04

Table 5. Input Test Vibration

Sinusoidal Test Conditions					
Direction	Frequency Range/Hz	5–8	8–80	80–100	
$X/Y/Z$	Acceleration	3.91 mm	3.5 g	1.5 g	
Random test vibration (Along X, Y, Z Direction)					
Frequency Range/Hz	20–60	60–200	200–300	300–800	800–2000
PSD(g2/Hz) (GRMS)	+3 dB/oct	0.0162	-8.156 3	0.0054	+3 dB/oct

Table 6. Comparison Between Test Results and Analysis Results

The Comparison of Modal Data						
	Analysis	Testing	Error			
1st Mode in X Direction	100.4H	97.2 Hz	3.3%			
1st Mode in Y Direction	102.3 Hz	100.9 Hz	1.5%			
1st Mode in Z Direction	124.3 Hz	117.2 Hz	6%			
The Comparison of Sinusoidal Data						
Direction	The response of mirror mounting point (g)					
	M2 mounting point			M4 mounting point		
	Analysis	Testing	Error	Analysis	Testing	Error
X	9.8	13.6	28%	10.4	13.7	24%
Y	13.8	14.3	3.5%	14.7	15	2%
Z	3.4	3.1	12%	3.6	3.3	11%
The Comparison of Random Vibration Data						
Direction	The response of mirror mounting point (GRMS)					
	M2 mounting point			M4 mounting point		
	Analysis	Testing	Error	Analysis	Testing	Error
X	7.4	8.1	8.6%	8.2	7.9	3.8%
Y	7.79	8.9	12.5%	8.16	8.9	8.3%
Z	21.4	26	17.6%	11.3	10.5	7.6%

relatively high tilt occurs in the θX direction while the effects of the temperature fluctuation and operation are relatively small. Finally, we can conclude from Table 4 that the results of the analysis and detection are all within our requirements.

B. Dynamic FEM Simulation Analysis and Vibration Tests

The dynamic FEM simulation analysis and vibration tests mainly verify the dynamic performance of the whole structure, including modal characteristics, sine acceleration response, and GRMS of random vibration. Table 5 gives the input test vibration of the space camera. Figure 11 shows the vibration test field. Table 6 gives the comparison between the test results and analysis results.

Fig. 11. Vibration test field.

According to the above tables, the errors of the FEM analysis and vibration test data are mostly less than 15%, with several data errors between 15% and 30%, which meet with the practical demands of the engineering. The first modal frequency of the space camera reaches up to 97.2 Hz, while the sine acceleration responses of the mirror mounting point are less than 15 g, and the GRMS of the random vibration is less than 26 GRMS. These all fit the design requirements. It is worth mentioning that the GRMS of the M4 mount point is 10.5 GRMS, much less than that of the M2 mount point (26 GRMS), which meets with the weighting factor specific value between α and β (nearly 2 : 1) mentioned in Section 3.B. Above all, the data has demonstrated the validity of the whole design and the optimization presented in this paper.

5. CONCLUSION

This paper has put forward a detailed structural design, an FEM simulation, and experimental verification of an off-axis TMA space camera with a long focal length and LFOV. Topology optimization of the main support structure was applied during the structural design stage. Compared with the traditional method, this paper takes the stiffness of the three axes into account, which led to a lighter structure and a higher natural frequency of the camera. A rod size optimization based on theoretical research of the random vibration response is proposed in this paper. The FEM analysis and experiments have verified the validity of the optimization. The research presented in this paper provides a meaningful method for large off-axis TMA space camera design.

Funding. National Natural Science Foundation of China (NSFC) (41501383).

REFERENCES

1. K. Zhang, N. Ruan, and D. Fu, "Analysis and consideration of development of oversea space off-axis TMA system camera," Spacecraft Recov. Remote Sens. **29**, 63–70 (2008), in Chinese.
2. Q. Geng and Z. Li, "CAE study on dynamic environments of the off-axis TMA multi-spectral remote sensor," in *International Conference on Transportation, Mechanical, and Electrical Engineering* (IEEE, 2011), pp. 2032–2035.
3. X. Gan, "Design for main support of long focal length space camera," in *International Conference on Mechtronic Science, Electric Engineering and Computer* (IEEE, 2011), pp. 515–518.
4. T. Bretdibat, V. Albouys, J. Berthon, N. Bouzou, P. Etcheto, and D. Laubier, "Tests of a high-resolution three-mirror anastigmat telescope," Proc. SPIE **3870**, 126–137 (1999).
5. B. Yang, "Characteristics and main specifications of IKONOS and QuickBird2 satellite camera-some points for developing such like satellite camera," Spacecraft Recov. Remote Sens. **23**, 14–16 (2002), in Chinese.
6. H. Imai, H. Katayama, T. Imai, and S. Suzuki, "Conceptual design of advanced land observing satellite-3," Proc. SPIE **7474**, 74740R (2009).
7. T. Iwata, H. Ishida, and Y. Osawa, "Advanced land observing satellite (ALOS): enabling technologies and platform performance," Proc. SPIE **7106**, 71060H (2008).
8. H. Imai, H. Katayama, T. Tadono, and S. Suzuki, "Outline of advanced land observing satellite-3 and its instruments," Proc. SPIE **8176**, 81760R (2011).
9. Y. An and J. Yao, "Application of carbon fibre reinforced plastic for optical camera structure," in *International Conference on Mechatronics and Automation* (IEEE, 2012), pp. 1928–1932.
10. D. Li, Q. Geng, and Z. Li, "Optimization design for main supporting structure of the off-axis TMA Space Remote Sensor," in *International Conference on Mechanic Automation and Control Engineering* (IEEE, 2010), pp. 252–254.
11. B. Atwood and T. P. O'Brien, "Adjustable truss for support, optical alignment, and athermalization of a Schmidt camera," Proc. SPIE **4841**, 403–410 (2003).
12. H. Xin and Z. Li, "Structural design for lightweight off-axis TMA space telescope," in *International Conference on Digital Manufacturing and Automation* (2011), pp. 1125–1128.
13. H. Xin and Y. Guan, "Design of main support of off-axis space remote sensor," Opt. Precis. Eng. **20**, 1258–1263 (2012), in Chinese.
14. L. Zhang and G. Jin, "Design and optimization of trussed supporting structure for off-axis three-mirror reflective space camera," Opt. Precis. Eng. **17**, 603–608 (2009), in Chinese.
15. C. Li and X. He, "Design and optimization of trussed structure for space camera based on Rayleigh algorithm," Infrared Laser Eng. **41**, 2405–2409 (2009), in Chinese.
16. S. Liu, R. Hu, and Q. Li, "Topology optimization-based lightweight primary mirror design of a large-aperture space telescope," Appl. Opt. **53**, 8318–8325 (2014).
17. U. Qy, W. Wang, B. Liu, and X. Li, "Topology optimization design of space rectangular mirror," Proc. SPIE **10154**, 1015421 (2016).
18. Q. Sun, "Topology optimization of support structure of multiwaveband imaging system," Opt. Eng. **54**, 115113 (2015).
19. M. Bendse and O. Sigmund, *Topology Optimization: Theory, Method and Applications* (Springer, 2003), Chap. 1.
20. Z. Han and G. Qu, "Wide-band random vibration response prediction study of the spacecraft structure," Chin. Space Sci. Technol. **1**, 24–30 (2002), in Chinese.
21. S. S. Rao, *Mechanical Vibrations* (Tsinghua University, 2009).
22. Y. Zou, Q. Wu, D. Dong, H. Liu, and H. Jia, "Research on analysis and test of random vibration on tripodic supporting structure of space camera," J. Syst. Simul. **16**, 5009–5017 (2009), in Chinese.